Study of fully submerged point absorber wave energy converter - modelling, simulation and scaled experiment

Boyin Ding*, Leandro Souza Pinheiro da Silva, Nataliia Sergiienko, Fantai Meng, Jonathan David Piper, Luke Bennetts, Markus Wagner, Benjamin Cazzolato, Maziar Arjomandi

Ocean Wave Energy Research Group, Faculty of Engineering, Computer and Mathematical Sciences, the University of Adelaide, South Australia, Australia

*boyin.ding@adelaide.edu.au

1. INTRODUCTION

Ocean waves are a huge resource of renewable energy. Wave energy converter (WEC) devices are being developed to optimise capture of this energy. A point absorber (PA), whose dimensions are much smaller than a wavelength, is a typical type of WEC with the main advantage being its insensitivity to wave direction. Examples of operational PA devices are the Carnegie CETO and Wavebob. PAs normally float on the water surface since wave power decreases with increasing submergence depth of the device (Falnes, 2002). However, there is an increasing trend to keep PAs fully submerged in order to increase the survivability of the device under extreme weather conditions. Sergiienko et al. (2017) undertook a systematic comparison study on floating and fully submerged PAs based on numerical simulations, which demonstrates that fully submerged PAs have the potential to capture a large amount of power from surge motion of the buoy component, twice as much as the power captured from heave motion of the buoy, whereas floating PAs capture power purely from heave motion of the buoy. This unique characteristic allows fully submerged PAs to capture the equivalent amount of wave energy to floating devices while maintaining high survivability.

High expenditures arise from manufacturing, installation, maintenance, and testing of the full-scale WECs in the open sea. Therefore, prior to the design and commissioning of the full-scale devices, numerical simulations and scaled experiments in wave tanks are required to prove design and control concepts, as well as to estimate their economic efficiencies. Modelling of hydrodynamics resulting from wave-body interaction is fundamental for the numerical simulation of point absorber WECs. Linear wave theory, based on the assumption of small wave amplitudes, is the most popular method to model hydrodynamics due to its high computational efficiency. The computed hydrodynamics of the PA can then be assembled in the frequency-domain. The resulting frequency-domain model can only be used to simulate the behaviour of the PA under regular wave conditions and does not have the capability to model nonlinearities such as drag forces and nonlinear power-take-off (PTO) forces. Alternatively, the hydrodynamics can be substituted into the Cummins equation (Cummins, 1962), a deterministic solution originally developed to investigate ship dynamics in the time-domain. The resulting time-domain model is able to include nonlinear forces and can be used for simulation under both regular and irregular wave conditions. However, it is more computationally expensive than the frequency-domain model. A spectral-domain model has recently been applied to WECs due to its high efficiency in solving nonlinear hydrodynamic problems. It is a probabilistic model of the system dynamics, which uses a statistical representation of the waves, and when passed through an appropriate transformation function produces a probabilistic estimate of the WEC response (Folley, 2010). The principle advantage of using a spectral-domain model over the conventional Cummins models is that for complex nonlinear systems it is computationally more efficient at providing estimates of power absorption under irregular waves.

In addition to numerical simulation, scaled experiments are also used to quantify the performance of WECs. There are few world-class wave tank testing facilities for WECs around the world. Examples are FloWave at the University of Edinburgh, Scotland; Model Test Basin at the Australian Maritime College, Australia; Ocean Engineering Water Tank at Shanghai Jiao Tong University, China; and Wave Basin at Indian Institute of Technology Madras, India. These facilities are normally developed for testing ship dynamics and offshore structures, and therefore are not always available for the testing of WECs. In addition, these facilities are often expensive to access, which is not affordable for many WEC research groups.

Besides discussing and benchmarking the typical tools for the study of fully submerged point absorber WECs, this paper has two main original contributions. Firstly, the spectral-domain model is applied to a fully submerged PA with numerical validation. Secondly, cost-effective scaled experiments are proposed and investigated for a fully submerged PA within a standard wave flume facility. The methods developed in this work could be applied to study floating PAs and even other types of WECs.

2. MATHEMATICAL MODELLING

In this study, a fully submerged PA is considered and the nonlinear force considered in modelling is the quadratic drag force. The PA dynamic equation takes the following form in the frequency-domain:

$$\Big(j\omega\big(\mathbf{M}+\mathbf{A}(\omega)\big)+\mathbf{B}(\omega)\Big)\hat{\boldsymbol{x}}=\hat{\mathbf{F}}_e(\omega)+\hat{\mathbf{F}}_b+\hat{\mathbf{F}}_{pto}, \tag{1}$$

where $\mathbf{M}$ is the mass matrix of the buoy; $\mathbf{A}(\omega)$ and $\mathbf{B}(\omega)$ are the hydrodynamic added mass and radiation damping matrices, which vary with wave frequency ω; $\hat{\mathbf{F}}_e(\omega)$ is the wave excitation force, which is also frequency dependent; $\hat{\mathbf{F}}_b$ is the net buoyancy force; $\hat{\mathbf{F}}_{pto}$ is the PTO control force; $\hat{\boldsymbol{x}}$ is the buoy velocities in heave, surge, and pitch under the assumption of plane incident waves. The hydrodynamic terms $\mathbf{A}(\omega)$, $\mathbf{B}(\omega)$ and $\hat{\mathbf{F}}_e(\omega)$ can be solved using boundary element solvers (e.g. WAMIT, ANSYS AQWA, NEMOH) for specific buoy shapes. For generic buoy shapes (e.g. sphere and cylinder), the coefficients can be solved using an analytical model developed by Srokosz (1979) and Jiang et al. (2014).

The Cummins equation takes the following form in the time-domain:

$$\big(\mathbf{M}+\mathbf{A}(\infty)\big)\ddot{\boldsymbol{x}}(t)+\int_0^t\mathbf{B}(t-\tau)\,\dot{\boldsymbol{x}}(t)d\tau=\mathbf{F}_e(t)+\mathbf{F}_b(t)+\mathbf{F}_{pto}(t)+\mathbf{F}_d(t), \tag{2}$$

where $\mathbf{A}(\infty)$ is the infinite-frequency added mass matrix ($\mathbf{A}(\omega)$ for $\omega=\infty$); $\int_0^t\mathbf{B}(t-\tau)\,\dot{\boldsymbol{x}}(t)d\tau$ represents the memory effect of the radiation force, which can be approximated as a transfer function and solved by using a Matlab toolbox developed by Perez and Fossen (2009). The wave excitation force time series $\mathbf{F}_e(t)$ can be calculated for both regular waves at a single frequency ω and irregular waves based on wave spectra models. Typical wave spectra models are JONSWAP, Bretschneider and Pierson-Moskowitz; $\mathbf{F}_d(t)$ is the quadratic nonlinear drag force that takes the form $\frac{1}{2}\rho C_d A|\dot{x}|\dot{x}$ on each dimension, where ρ is the density of seawater, C_d is the drag coefficient usually determined from experiments for particular buoy shapes, and A is the cross-sectional area of the buoy perpendicular to the motion direction.

The spectral-domain model is formulated using the same construction as the frequency-domain model and the response of the PA at each wave frequency can be obtained from (Folley, 2010)

$$\Big(j\omega_i\big(\mathbf{M}+\mathbf{A}(\omega_i)\big)+\big(\mathbf{B}(\omega_i)+\mathbf{G}(\omega_i)\big)\Big)\hat{\boldsymbol{x}}_i=\hat{\mathbf{F}}_e(\omega_i)+\hat{\mathbf{F}}_b+\hat{\mathbf{F}}_{pto}, \tag{3}$$

where $\mathbf{G}(\omega_i)$ is the quasilinear drag coefficients linearised from the quadratic nonlinear drag force and takes the form $2C_d\sqrt{\frac{1}{\pi}\sum_i\omega_i^2|x_i|^2}$ on each dimension. The response of the PA at each frequency is dependent not only on hydrodynamic coefficients at that frequency, but also the response of the PA at all frequencies due to the nonlinear force. Total response under irregular waves can then be calculated by superposition of all the wave components. There is no known analytical solution to the spectral-domain model, so an iterative solver has to be used to estimate the response of the PA for the estimation the quasilinear drag coefficients.

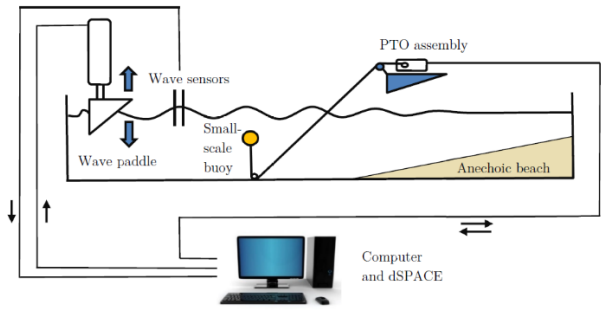

Figure 1. Scaled experiment set-up in the wave flume

Figure 2. Buoy assembly (0.136m diameter sphere)

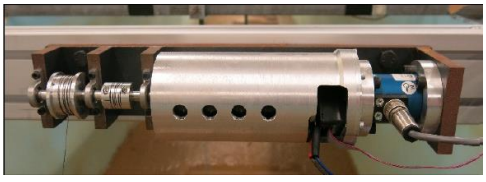

Figure 3. PTO assembly (from left to right: rope spool, shaft coupling, motor-encoder-housing, torque sensor)

3 SMALL-SCALE EXPERIMENT

Figure 1 shows the set-up of the scaled experiment in a standard wave flume facility located in the Chapman lab within the University of Adelaide, which is 32m long, 1.3m wide and 1m deep. A piston-type hydraulic-driven wave paddle is placed at the upstream end of the flume. The up and down motion of the wave paddle generates propagating waves. A perforated anechoic beach sits at the downstream end of the flume, which is used to prevent waves from reflecting back. A fully submerged PA is placed at 5m downstream of the wave paddle, where the generated waves demonstrate the desired regularity. A small boat pulley is placed at the bottom of the flume forming a mooring point. The PA is anchored via a high strength fishing line, which goes through the pulley and rolls on the rope spool within a custom-built PTO system. Six custom-built wave probes are placed around the PA to monitor surrounding wave conditions, two upstream, two downstream, and two at the sides. A DS1104 dSPACE controller is coded via Matlab to control the wave conditions generated by the paddle based on the wave probe readings, as well as control the PTO system to apply desired force on the PA. It also collects data from wave probes, IMU, and motor for post-processing.

Figure 2 shows the buoy assembly of the PA, whose shell is 3D printed from VisiJet M3. The inner space of the buoy shell is used to place an IMU (LORD MicroStrain 3DM-GX4-25) that measures buoy movements and additional weights that allow the change of the net buoyancy and the centre of gravity of the buoy. The shell of the buoy is closed via screw fixation and sealed by double O-rings. The IMU cable exits the buoy shell via a cable gland fixed at the top of the shell. A U tunnel profile is printed at the bottom of the buoy shell, forming an anchoring point for the tether. The dimension of the 3-D printed buoy (0.136m diameter) is 1/73.5 of the full-scale buoy (10m diameter) so that the blockage ratio of the buoy to the flume width is less than 12%. A higher blockage ratio has the risk of modifying the scattering force on the buoy. The ratio (1/73.5) was also chosen considering the similarity of drag coefficients between small/full scales.

Figure 3 shows the PTO assembly that is used to emulate any PTO behaviour. A Maxon RE50 motor drives a rope spool via a shaft coupling and consequently applies PTO force to the PA via pulley-tether coupling. The shafts of the rope spool and motor sit on three rolling-element bearings fixed to the base. The housing of the motor is attached to the base via an aluminium shell and a Lorenz Messtechnik GmbH D-2209 torque sensor. The torque sensor measures the torque applied by the motor. A motor encoder measures the tether displacement. The motor is selected to generate sufficient PTO force to overcome the buoy net buoyancy force and the Coulomb friction force within the PTO assembly, as well as to generate the desired PTO force. Assuming generic linear spring-damper control, the torque command for the motor takes the following form:

$$T_m = -(\rho V - m)g \cdot r + \text{sign}(\dot{\theta}) \cdot c_c + k_{pto} \cdot \theta \cdot r^2 + c_{pto} \cdot \dot{\theta} \cdot r^2, \quad (4)$$

where V is the displaced water due to the buoy; m is the buoy mass; g is the gravitational acceleration; r is the radius of the rope spool; θ is the angular displacement of the motor; c_c is the Coulomb friction coefficient of the PTO assembly; k_{pto} is the scaled PTO spring stiffness; c_{pto} is the scaled PTO damping coefficient. From Eq. 4, it can be seen that the selection of the rope spool radius r compromises the maximum required motor torque and the magnitude of the Coulomb friction torque within the total required motor torque. A current feedback control is applied to track the desired motor torque command calculated from Eq. 4, in order to achieve a desired spring-damper behaviour. Since there is noise within $\dot{\theta}$ arising from differentiating the encoder reading, $\text{sign}(\dot{\theta}) \cdot c_c$ is replaced by a relay function and a low pass filter is applied to remove noise within $\dot{\theta}$ for PTO damping control. The selection of the filter cut-off frequency compromises the phase delay introduced into damping control and the noise attenuation capability.

4. RESULTS

A benchmark study has been undertaken between the modelling methods and the scaled experiment under both regular and irregular wave conditions. Table 1. summarises the full-scale PA and scaled PTO properties.

Table 1. Configuration for the benchmark study

PA property (sphere buoy)	**Values**	**Wave property** (Pierson-Moskowitz spectra used)	**Values**	**PTO property** (for 1/73.5 scale ratio)	**Values**
Water depth	48m	Wave amp (regular)	1.5m	Filter cut-off frequency	50Hz
Buoy radius	5m	Wave period	7, 9, 12s	Relay threshold	eps in Matlab
Submergence depth	8m	Wave height (irregular)	3m	r	15mm
Mass to buoyancy ratio	0.5	Energy wave period	7, 9, 12s	c_c	0.012Nm

Before conducting testing in the wave flume, the buoy was attached to the PTO system without interacting with water to validate the control performance of the PTO system. A decay testing was undertaken by realising the buoy 50mm away from its equilibrium position under spring-damper control. It was evident that the buoy oscillates around its natural frequency $\sqrt{k_{pto}/m}$ and the oscillation decays exponentially almost under the defined PTO damping, c_{pto}. In addition, the hydrodynamic coefficients of the scaled buoy were measured from wave flume experiment, which are similar to the ones computed from linear wave theory, with errors within 20%.

Figure 4 shows the power outputs of the PA resulting from the frequency-domain model (Eq. 1), the time-domain model (Eq. 2) and the scaled experiment under regular wave conditions (power averaged over 16 runs for each wave period, where power in each run averaged over 30 wave periods). The PTO spring and damper were optimised for each wave period subjected to a buoy motion constraint of 3m using the frequency-domain model. The frequency-domain model overestimates the power absorption efficiency of the PA because the nonlinear drag force is not considered. The time-domain model gives much closer results to the experiments, with errors within 10%. Figure 5 shows the power outputs of the PA resulting from the time-domain model (Eq. 2) and the spectral-domain model (Eq. 3) under irregular wave conditions, averaged over 300 peak wave periods (experimental data under irregular waves are still under investigation). The PTO spring and damper were optimised for each energy wave period. The spectral-domain model results match the time-domain model results reasonably well, with errors within 10%.

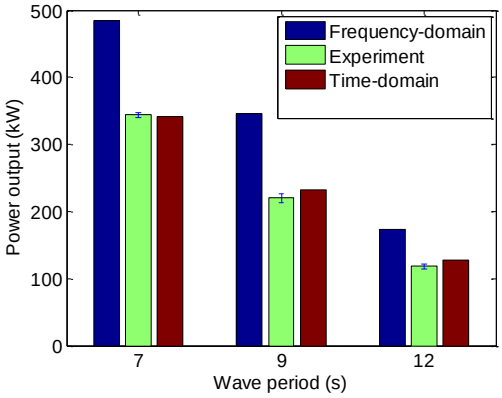

Figure 4. Power outputs under regular waves

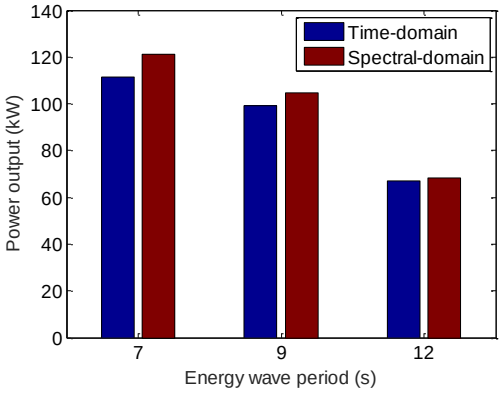

Figure 5. Power outputs under irregular waves

5. CONCLUSION

- We successfully applied a spectral-domain model to fully submerged PA WECs with numerical validation against the conventional time-domain nonlinear model.
- The proposed cost-effective scaled experiment demonstrated high fidelity against the time-domain model, with errors increasing with the increase of wave period. Under long waves, high PTO damping was required to keep the buoy fully submerged, leading to slow tether motion, where the parasitic loss in the PTO assembly cannot be properly compensated.
- More experimental studies are being undertaken to understand the optimal control solution to compensate for parasitic loss within the set-up, especially when the tether motion is slow. One potential solution that will be investigated is the use of dither signals.

REFERENCES

Falnes, J., 2002, Ocean Waves and Oscillating Systems: Linear interactions including Wave-Energy Extraction (Cambridge University Press).

Sergiienko, N.Y. et al., 2017. Performance comparison of the floating and fully submerged point absorber wave energy converters. Renew. Energy, accepted.

Cummins, W.E., 1962. The impulse response function and ship motions. Schiffstechnik, 9, 101-109.

Folley, M. et al., 2010. Spectral modelling of wave energy converters, Coastal Eng. 57, 892-897.

Srokosz, M.A., 1979. The submerged sphere as an absorber of wave power. J. Fluid Mech. 95, 717-741.

Jiang S., 2014. Analytial solution of a wave diffraction problem on a submerged cylinder. J. Eng. Mech. 140, 225-232.

Perez, T. et al., 2009. A Matlab toolbox for parametric identification of radiation-force model of ships and offshore structures. J, Model. Identif. Control, 30, 1-15.